Fabrication of Microchip Devices for Organ-on-a-Chip and Lab- on- a-Chip Applications

CNF Project Number: 2857-19

Principal Investigator(s): Esak (Isaac) Lee

User(s): Wukun Ouyang, Renhao Lu, Yansong Peng

Affiliation(s): Meining School of Biomedical Engineering, Cornell University Primary Source(s) of Research Funding: R01 CA279560; R01 HL165135

Contact: el767@cornell.edu, wo55@cornell.edu, rl839@cornell.edu, yp255@cornell.edu

Research Group Website: https://leelab.bme.cornell.edu/

Primary CNF Tools Used: Heidelberg DWL2000 Mask Writer, ABM Contact Aligner, MVD100, SU-8 hotplate

Abstract:

Organ-on-a-chip is a microfluidic cell culture platform, integrated circuit (chip) that simulates the activities, mechanics, and physiological response of an entire organ or an organ system. Our lab aims to create organ-on-a-chip devices to study the mechanism of various diseases. In the past year, we mainly focused on three projects: (1) Astrocyte-driven vasoconstriction impairs glymphatic clearance in a human tauopathyon-chip model; (2) Monomeric and oligomeric amyloid-β cause distinct Alzheimer's disease pathophysiological characteristics in astrocytes in human glymphatics-on-chip models; (3) Three-Dimensional Lymphatics-on-a-Chip Distinct, Size-Dependent Nanoparticle Transport Mechanisms in Lymphatic Drug Delivery.

Summary of Research:

Project 1: Astrocyte-driven vasoconstriction impairs glymphatic clearance in a human tauopathy-on-chip model [1]

The glymphatic system is a critical pathway for clearing metabolic waste from the brain by mediating cerebrospinal fluid and interstitial fluid exchange. In Alzheimer's disease (AD), tau protein accumulation is strongly associated with impaired glymphatic clearance, yet the underlying mechanism remains poorly defined. In this study, we employed a three-dimensional human glymphatics-on-chip model to investigate fluid transport and mass clearance in a brain-mimetic extracellular matrix containing engineered blood vessels (BV) surrounded by primary astrocytes. We found that phosphorylated tau (p-tau) induced morphological transformation of astrocytes into a hypertrophic, hypercontractile state, leading to astrocyte-mediated vasoconstriction and impaired glymphatic clearance. Notably, p-tau did not affect blood endothelial cells directly, implicating astrocyte-dependent mechanisms in glymphatic deregulation. Pharmacological inhibition of nonmuscle myosin II with blebbistatin reversed

astrocytic hypercontractility, restored BV diameters, and rescued glymphatic function. These findings elucidate a glial-specific mechanism of tau-induced glymphatic dysfunction and underscore astrocytic contractility as a promising therapeutic target in AD.

Project 2: Monomeric and oligomeric amyloid-\(\beta \) cause distinct Alzheimer's disease pathophysiological characteristics in astrocytes in human glymphatics-on-chip models [2]

Alzheimer's disease (AD) is marked by the aggregation of extracellular amyloid- β (A β) and astrocyte dysfunction. For A β oligomers or aggregates to be formed, there must be A β monomers present; however, the roles of monomeric $A\beta$ (mA β) and oligomeric A β (oA β) in astrocyte pathogenesis are poorly understood. We cultured astrocytes in a brain-mimicking three-dimensional (3D) extracellular matrix and revealed that both mAβ and oAβ caused astrocytic atrophy and hyperreactivity, but showed distinct Ca2+ changes in astrocytes. This 3D culture evolved into a microfluidic glymphatics-onchip model containing astrocytes and endothelial cells with the interstitial fluid (ISF). The glymphatics-on-chip model not only reproduced the astrocytic atrophy, hyper-reactivity, and Ca2+ changes induced by mAβ and oAβ, but recapitulated that the components of the dystrophin-associated complex (DAC) and aquaporin-4 (AQP4) were properly maintained by the ISF, and dysregulated by mAβ and oAβ. Collectively, mAβ and oAβ cause distinct AD pathophysiological characteristics in the astrocytes.

Project 3: Three-Dimensional Lymphatics-on-a-Chip Reveals Distinct, Size- Dependent Nanoparticle Transport Mechanisms in Lymphatic Drug Delivery

Although nanoparticle-based lymphatic drug delivery systems promise better treatment of cancer, infectious disease, and immune disease, their clinical translations are limited by low delivery efficiencies and unclear transport mechanisms. Here, we employed a three-dimensional (3D) lymphatics-on-a-chip featuring an engineered lymphatic vessel (LV) capable of draining interstitial fluids including nanoparticles. We tested lymphatic drainage of different sizes (30, 50, and 70 nm) of PLGA-b-PEG nanoparticles (NPs) using the lymphatics-on-a-chip device. In this study, we discovered that smaller NPs (30 and 50 nm) transported faster than larger NPs (70 nm) through the interstitial space,

as expected, but the smaller NPs were captured by lymphatic endothelial cells (LECs) and accumulated within their cytosol, delaying NP transport into the lymphatic lumen, which was not observed in larger NPs. To examine the mechanisms of sizedependent NP transports, we employed four inhibitors, dynasore, nystatin, amiloride, and adrenomedullin, to selectively block dynamin-, caveolin-, macropinocytosis-mediated endocytosis-, and cell junction-mediated paracellular transport. Inhibiting dynamin using dynasore enhanced the transport of smaller NPs (30 and 50 nm) into the lymphatic lumen, minimizing cytosolic accumulation, but showed no effect on larger NP transport. Interestingly, the inhibition of caveolin by nystatin decreased the lymphatic transport of larger NPs without affecting the smaller NP transport, indicating distinct endocytosis mechanisms used by different sizes of NPs. Macropinocytosis inhibition by amiloride did not change the drainage of all sizes of NPs; however, paracellular transport inhibition by adrenomedullin blocked the lymphatic transport of NPs of all sizes. We further revealed that smaller NPs were captured in the Rab7-positive late-stage lymphatic endosomes to delay their lymphatic drainage, which was reversed by dynamin inhibition, suggesting that Rab7 is a potential target to enhance the lymphatic delivery of smaller NPs. Together, our 3D lymphatics-on-a-chip model unveils sizedependent NP transport mechanisms in lymphatic drug delivery.

References:

- [1] Park R, Peng Y, Yslas AR, Lee E. Astrocyte-driven vasoconstriction impairs glymphatic clearance in a human tauopathy-on-chip model. APL Bioeng. 2025 Jun 16;9(2):026126. doi: 10.1063/5.0261875. PMID: 40530247; PMCID: PMC12173474.
- [2] Yslas AR, Park R, Nishimura N, Lee E. Monomeric and oligomeric amyloid-β cause distinct Alzheimer's disease pathophysiological characteristics in astrocytes in human glymphatics-on-chip models. Lab Chip. 2024 Aug 6;24(16):3826-3839. doi: 10.1039/d4lc00287c. PMID: 39037244; PMCID: PMC11302770.
- [3] Lu R, Lee BJ, Lee E. Three-Dimensional Lymphatics-on-a-Chip Reveals Distinct, Size-Dependent Nanoparticle Transport Mechanisms in Lymphatic Drug Delivery. ACS Biomater Sci Eng. 2024 Sep 9;10(9):5752-5763. doi: 10.1021/acsbiomaterials.4c01005. Epub 2024 Aug 23. PMID: 39176471.

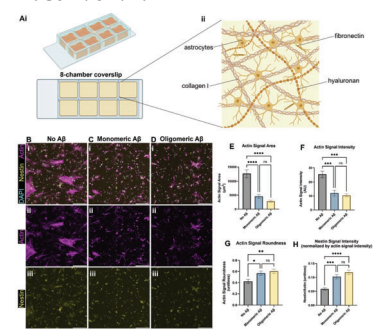


Figure 2: Astrocytic atrophy and reactivity changes in astrocytes exposed to monomeric and oligomeric $A\beta$. (A) A schematic of our initial 3D culture of astrocytes. (Ai) Human astrocytes were cultured in 3D ECM in chambers on a glass coverslip, (Aii) with brain-mimicking ECM components including collagen I, hyaluronan, and fibronectin. (B) Immunostaining astrocytes with phalloidin (F-actin staining), anti-nestin antibodies, and DAPI. The astrocytes were exposed to either no $A\beta$ (B), monomeric (C), or oligomeric $A\beta$ (D). (E) Changes in actin signal area per cell by monomeric or oligomeric $A\beta$. (F) Changes in total actin signal intensity by monomeric or oligomeric $A\beta$. (G) Changes in roundness by monomeric or oligomeric $A\beta$. (H) Changes in astrocytic reactivity by monomeric or oligomeric $A\beta$. (H) Changes in astrocytic reactivity by monomeric or oligomeric $A\beta$, as measured by nestin signal intensity relative to actin signal intensity. Scale bars $(B-D)=200~\mu m$. * (p<0.05), *** (p<0.01), **** (p<0.001) indicate statistical significance. ns=not significant.

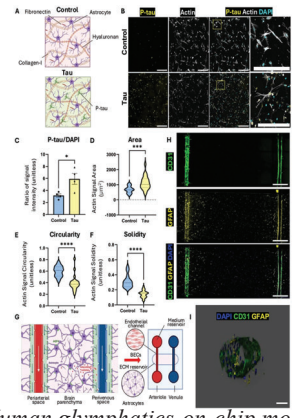


Figure 1: Human glymphatics-on-chip model recapitulates 3D neurovascular architecture with astrocytic reactivity to tau. (a) A schematic representation of the ECM components (astrocytes, fibronectin, collagen I, and hyaluronan) and experimental groups (control, red; tau-treated, green). (b) Immunofluorescence staining of phosphorylated tau (p-tau, yellow), actin (gray), and nuclei (DAPI, cyan) in control and tau-treated astrocytes. Zoomed insets highlight structural changes. (c) Quantification of p-tau signal intensity, normalized to DAPI (N¼ 4). (d) Violin plot showing astrocyte area under control and tau-treated conditions (N¼ 30-40). (e) Violin plot representing astrocyte circularity ($N\frac{1}{4}$ 30–40). (f) Violin plot for astrocyte solidity, showing reduced compactness in tau-treated astrocytes (N¼ 30–40). (g) A schematic of the in vivo glymphatic system alongside the glymphatics-on-chip platform, depicting the arrangement of astrocytes and blood vessel channels. (h) Immunofluorescence images showing endothelial marker CD31 (green), astrocytic marker GFAP (yellow), and DAPI (blue) within the glymphatics-on-chip platform. (i) A representative, 3D-rendered blood vessel surrounded by astrocytes. Scale bars: 300 lm (b), 1 mm (h), and 100 lm (i). Statistical significance: (p < 0.05), (p < 0.001), and (p < 0.0001).

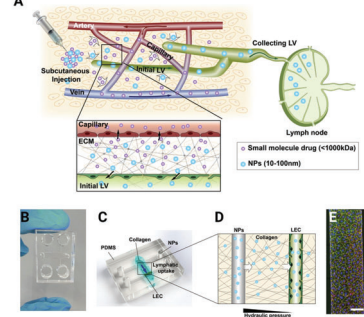


Figure 3: 3D lymphatics-on-a-chip modelto decipher size-dependent nanoparticle (NP) transportinto lymphatic vessels (LVs). (A) Schematic of the NP drug delivery system. Upon subcutaneous injection, water-soluble molecules $(\stackrel{<}{<} 1000 \text{ kDa})$ are collected by the blood capillary; however, NPs(10-100nm) are preferably drained into the lymphatic vessels via their permeable junctions and reach draining lymph nodes. (B,C) Picture and schematic of the lymphaticson-a-chip model. The collagen bulk (blue) represents the 3D interstitial space, with ECM proteins penetrated by two hollow channels. (D) One of the channels seeded with lymphatic endothelial cells (LECs) forms an engineered LV. The second, cell-free channel allows the introduction of excess fluid to form an interstitial fluid pressure gradient between the acellular and lymphatic channels. Simulating subcutaneous NP injection, excess media, including NPs, are loaded into the acellular channel. NPs transport through the interstitial ECM space, reach the engineered LV, and drain into the LV. Drained and remaining NPs are collected from the 4 circular reservoirs for analysis. (E) Representative image of an engineered LV stained with anti-VE-cadherin (adherens junction, green) antibodies, phalloidin (F-actin, red), and DAPI (nucleus, blue). Scale bar in (E): 100 μm.